Cell

The Structure of the Phage T4 DNA Packaging Motor Suggests a Mechanism Dependent on Electrostatic Forces

Siyang Sun,[1,3] Kiran Kondabagil,[2,3] Bonnie Draper,[2] Tanfis I. Alam,[2] Valorie D. Bowman,[1] Zhihong Zhang,[2] Shylaja Hegde,[2] Andrei Fokine,[1] Michael G. Rossmann,[1,*] and Venigalla B. Rao[2,*]
[1]Department of Biological Sciences, Purdue University, 915 W. State Street, West Lafayette, IN 47907-2054, USA
[2]Department of Biology, The Catholic University of America, 620 Michigan Avenue NE, Washington, DC 20064, USA
[3]These authors contributed equally to the work
*Correspondence: mr@purdue.edu (M.G.R.), rao@cua.edu (V.B.R.)
DOI 10.1016/j.cell.2008.11.015

SUMMARY

Viral genomes are packaged into "procapsids" by powerful molecular motors. We report the crystal structure of the DNA packaging motor protein, gene product 17 (gp17), in bacteriophage T4. The structure consists of an N-terminal ATPase domain, which provides energy for compacting DNA, and a C-terminal nuclease domain, which terminates packaging. We show that another function of the C-terminal domain is to translocate the genome into the procapsid. The two domains are in close contact in the crystal structure, representing a "tensed state." A cryo-electron microscopy reconstruction of the T4 procapsid complexed with gp17 shows that the packaging motor is a pentamer and that the domains within each monomer are spatially separated, representing a "relaxed state." These structures suggest a mechanism, supported by mutational and other data, in which electrostatic forces drive the DNA packaging by alternating between tensed and relaxed states. Similar mechanisms may occur in other molecular motors.

INTRODUCTION

Most bacteriophages and many eukaryotic viruses assemble empty procapsids into which the genome is subsequently packaged, thereby compressing a large amount of negatively charged DNA into a limited space (Black, 1989; Rao and Feiss, 2008). The process of translocating DNA into the viral capsid is powered by ATP hydrolysis and is driven by a packaging motor that is located at a unique 5-fold vertex of the icosahedral capsid (Figures 1A and 1B). Hydrolysis of one ATP molecule can translocate, on average, two base pairs into the procapsid of the tailed phages ϕ29 (Guo et al., 1987) and T3 (Morita et al., 1993). Because the proteins of the DNA packaging motor in tailed phages have sequence and structural similarities, it is probable that they will also have similar mechanisms and, thus, presumably consume one ATP to translocate two base pairs. Viral genome packaging motors can generate forces of about 60 picoNewtons, which is about 20 times the force generated by myosin motors, placing them among the most powerful molecular machines (Chemla et al., 2005; Fuller et al., 2007; Smith et al., 2001). Upon completion of packaging, the DNA packaging motor is released and the separately assembled tail is attached to produce the mature infectious viral particle.

In tailed DNA bacteriophage T4, the packaging motor consists of the dodecameric 61 kDa portal protein, gene product 20 (gp20), and a "terminase" complex consisting of the 70 kDa large terminase protein, gp17, and the 18 kDa small terminase protein, gp16 (Rao and Black, 2005). The stoichiometries of both gp17 and gp16 are unknown. The N-terminal domain (amino acids 1–360) of gp17 has ATPase activity and the C-terminal domain (amino acids 361–610) has nuclease activity (Kanamaru et al., 2004). These two functional domains need to be physically linked in order for DNA packaging to occur (Kondabagil et al., 2006). The ATPase activity of gp17 or the N-terminal domain of gp17 on its own is low. However, addition of gp16 stimulates gp17's ATPase activity ("gp16-stimulated ATPase activity") by about 50-fold (Leffers and Rao, 2000). ATPase activity can also be stimulated by DNA translocation when gp17 is associated with the procapsid ("packaging ATPase activity") (Kondabagil et al., 2006). T4 replicates its genome as a head-to-tail concatemer and packages 1.02 genomes per capsid, with different ends for each mature viral particle (Streisinger et al., 1967). The function of the nuclease activity is to cut the concatemer at the beginning of DNA packaging and again at the end after the viral genome is packaged. When the head is full, a "headful" signal is presumably transmitted to gp17, causing gp17 to cleave the DNA and to disassociate from the filled head.

The only known crystal structures of portal assemblies are for phages ϕ29 and SPP1 (Simpson et al., 2000; Lebedev et al., 2007). Cryo-electron microscopy (cryo-EM) studies of phages ϕ29 (Simpson et al., 2000), SPP1 (Orlova et al., 2003), T4 (Leiman et al., 2004), P22 (Chang et al., 2006; Lander et al., 2006), and ε15 (Jiang et al., 2006) show that the wider end of the cone-shaped portal is inside the capsid, and the narrower end protrudes out of the capsid. Models for the mechanism of DNA translocation have been proposed on the basis of the symmetry mismatch of the capsid (5-fold), the portal (12-fold), and the 10_1 B-form structure of DNA (Hendrix, 1978). In these models, the portal is

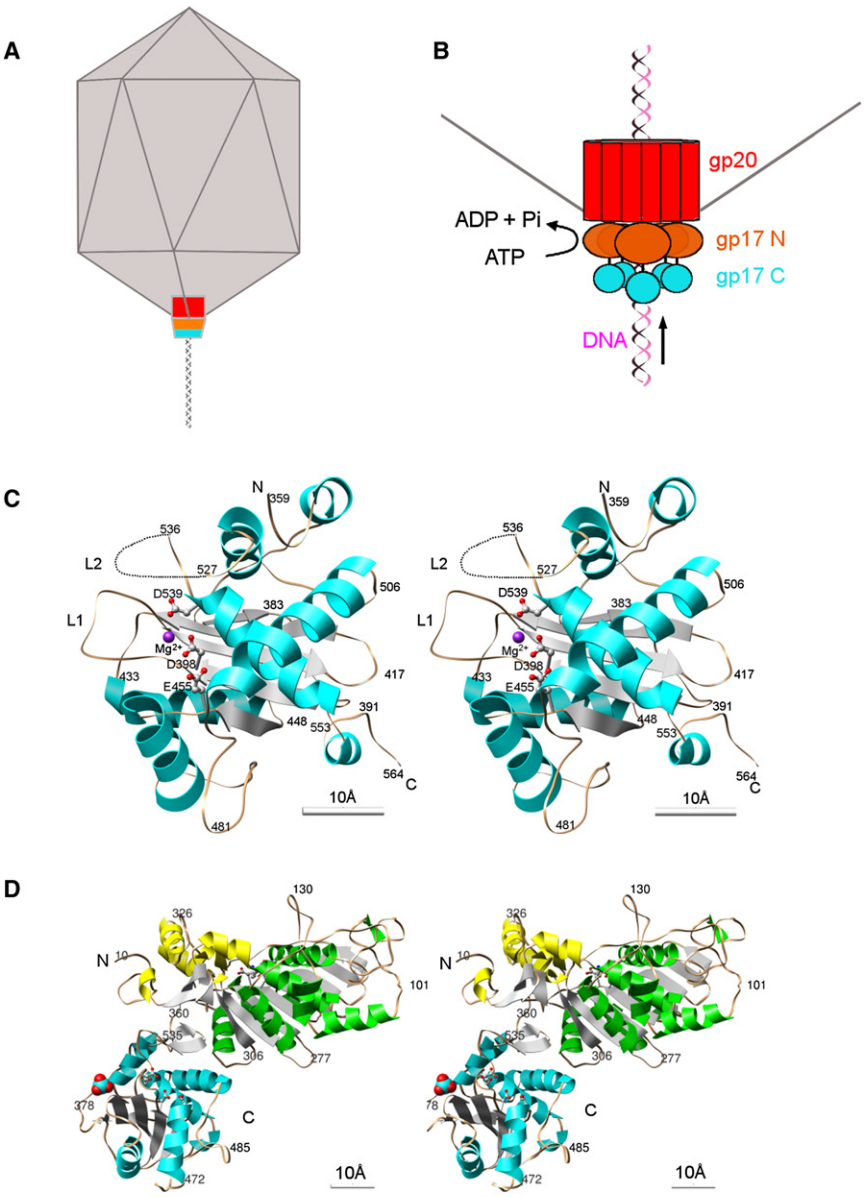

Figure 1. The Bacteriophage T4 DNA Packaging Machine

(A) The T4 procapsid during DNA packaging.

(B) The packaging motor consists of the dodecameric portal protein gp20 and the large terminase gp17. The gp17 molecule has an N-terminal domain (gp17 N), which hydrolyzes ATP, and a C-terminal domain (gp17 C), which has nuclease activity and a DNA translocation function.

(C) A stereo ribbon diagram of the RB49 gp17 C-terminal domain crystal structure with α helices colored in cyan, β sheets silver, and loops brown. The termini are labeled as N and C, and selected amino acids are numbered. A flexible loop L2, shown as a dotted line, was not seen in the electron density. A magnesium ion was detected in the electron density and is shown as a purple sphere. Conserved acidic residues are shown in ball-and-stick form.

(D) A stereo ribbon diagram of the T4 gp17 crystal structure with α helices colored green in the N-terminal subdomain I, yellow in the N-terminal subdomain II, and cyan in the C-terminal domain. The β sheets are colored silver, and loops are dark yellow. Selected amino acids are numbered. Catalytic residues in the ATPase and nuclease active centers are shown in ball-and-stick form, and a bound phosphate ion is shown as cyan and red spheres. The ribbon diagrams were generated with the Chimera program (Pettersen et al., 2004).

assumed to rotate while DNA is being translocated and ATP hydrolysis provides energy. However, it has been shown for both the T4 and ϕ29 phages that portal rotation is unlikely (Baumann et al., 2006; Hugel et al., 2007).

Crystallization of the T4 phage full-length large terminase protein gp17, the key component of the viral DNA packaging motor, has been difficult. Initially, we crystallized and then determined the structure of a mutant form of the T4 gp17 ATPase domain (D255E/E256D, "N360-ED") (Sun et al., 2007). Subsequently, we were able to crystallize the gp17 C-terminal domain fragment (amino acids 361–577) of bacteriophage RB49, a close relative of T4 (72% sequence identity), in which the final ten residues were disordered, suggesting that gp17 might be crystallizable if it were terminated at residue 567. Indeed, the shortened form of T4 gp17 (amino acids 1–567) could be crystallized when the ATPase active center had the D255E/E256D mutation. Here, we present these crystal structures and cryo-EM reconstructions of the T4 procapsid complexed with the gp17 motor and propose a mechanism for DNA packaging consistent with mutational as well as other biochemical and structural data.

RESULTS

The RB49 gp17 C-Terminal Domain Structure

The crystal structure of the RB49 gp17 C-terminal domain (Table 1) measured about 31 × 36 × 37 Å and consisted of a mixed, mostly antiparallel, β sheet sandwiched between α helices (Figure 1C). The Gly527-Gly535 loop (L2) was missing in the electron density. A spatially adjacent Glu401-Gln405 loop (L1) had weak density and was observed probably only because it made a crystal lattice contact.

Despite no detectable sequence identity, the RB49 gp17 C-terminal domain superimposed well onto the structures of the RNase H/resolvase/integrase superfamily, with the greatest similarity to RuvC resolvase (Table S1 available online). Three conserved acidic residues constitute the active center in the RNase H family of nucleases and are Asp, Asp, Asp in RNase H; Asp, Asp, Glu in transposases and retroviral integrases; and Asp, Glu, Asp in resolvase (Nowotny et al., 2005) (Figure S1). Two metal ions (Mg^{2+} or Mn^{2+}), coordinated by the conserved acidic residues, were found in the structure of RNase H

Table 1. Data Collection and Refinement Statistics

	RB49 gp17 C-Terminal Domain				T4 gp17
	Native	Hg Derivative	Native	Native	Native
Data Collection					
X-ray source	home	home	23-ID-B	23-ID-B	23-ID-B
Wavelength (Å)	1.5418	1.5418	1.0332	1.0332	1.0332
Resolution (Å)	1.6	2.3	1.16	2.2	2.8
Space group	$P2_12_12$	$P2_12_12$	$P2_12_12$	$C2$	$P6_222$
Unit cell (Å)	a = 52.6, b = 125.1, c = 37.2	a = 52.8, b = 124.8, c = 37.6	a = 52.6, b = 125.2, c = 37.2	a = 96.4, b = 126.7, c = 52.4, β = 106.0°	$a = b$ = 119.6, c = 226.3
Unique reflections	32,564	11,378	85,573	29,056	23,617
Average redundancy	4.6	6.6	5.8	3.1	2.6
I/σ[a]	48.1 (7.8)	35.6 (6.6)	41.2 (3.9)	34.8 (8.7)	23.3 (3.3)
Completeness (%)	97.6 (90.9)	97.5 (99.3)	99.4 (96.6)	95.0 (86.9)	96.8 (97.9)
R_{merge} (%)[b]	3.3 (21.8)	10.9 (41.4)	4.1 (38.4)	4.1 (13.9)	7.0 (34.9)
Phasing power[c]		1.821 (iso), 1.395 (ano)			
Refinement					
Resolution (Å)			1.16	2.8	2.8
$R_{working}$ (%)[d]			13.6 (24.4)	24.2 (33.2)	25.3 (33.6)
R_{free} (%)[e]			17.1 (26.5)	29.0 (38.7)	29.2 (41.0)
Average B factor (Å^2)			21.9	53.6	68.0
rmsd bonds (Å)			0.018	0.008	0.006
rmsd angles (°)			2.3	1.3	1.1
Ramachandran disallowed			0	0	0

[a] Values in parentheses throughout the table correspond to the last shell.
[b] $R_{merge}=\Sigma|I-<I>|/\Sigma I$, where I is measured intensity for reflections with indices hkl.
[c] Phasing power =[$|F_h(calc)|$/ phase-integrated lack of closure].
[d] $R_{working}=\Sigma||F_{obs}| - |F_{calc}||/\Sigma|F_{obs}|$.
[e] R_{free} has the same formula as $R_{working}$, except that calculation was made with the structure factors from the test set.

complexed with an RNA/DNA hybrid. A two-metal-ion mechanism was proposed for the catalytic function of this family of nucleases (Beese and Steitz, 1991), where one metal ion activates the hydroxyl nucleophile and the other stabilizes the pentacovalent phosphorane transition state. Asp398 and Glu455 of RB49 gp17 are structurally equivalent to the first and second conserved acidic residues in the RNase H family, respectively. The third conserved acidic residue is spatially variable within the family. Its location appears to be determined by the substrate and corresponds to Asp539 in RB49 gp17. A metal ion, as indicated by a strong density (over 7σ high), was coordinated by both Asp398 and Asp539. X-ray fluorescence in conjunction with the observed coordination geometry confirmed the metal ion to be Mg^{2+}. However, in the absence of bound substrate, there was no evidence for a second metal ion in the electron density. The three acidic metal ion ligands, Asp398, Glu455, and Asp539 in RB49 gp17, are strictly conserved in the phage terminases (Figure S2). Mutating any of the nuclease catalytic residues (D401N, E458A, and D542A) in full-length T4 gp17 results in a complete loss of nuclease activity, without affecting ATPase or DNA packaging activities (Alam et al., 2008; Rentas and Rao, 2003). Thus, the nuclease activity site is distinct from the DNA translocation site.

The nuclease active center in the RB49 gp17 C-terminal domain is in a groove about 20 Å in diameter, with its edges lined by positively charged amino acids, Arg403, Lys465, Lys487, Lys490, Arg491, Lys493, and Lys526. The shape and charge distribution of the groove are complimentary to the structure of B-form dsDNA, which suggests that this groove is where DNA binds and is cleaved when the head is full (Figure S3).

The T4 gp17 Structure

The T4 gp17 structure (amino acids 1–567 with the D255E/E256D mutation) was determined with the use of the T4 N-terminal and RB49 C-terminal domain structures as molecular replacement search models (Figure 1D, Table 1). The N- and C-terminal domain structures of the complete gp17 do not significantly differ to the structures of each domain alone and are connected by a conserved flexible linker region of amino acid sequence GTSGT (amino acids 358–362) (Figure S4). No ADP was observed in the electron density, although it had been included in the crystallization condition. This could be caused by a crystal lattice contact that displaces the Cys125-Arg140 loop that interacts with the adenine ring in the ATP or ADP bound structure of the N-terminal domain (Sun et al., 2007). No Mg^{2+} ion density was observed in the C-terminal nuclease active center. One inorganic phosphate coordinated by His385, His430, and His516 was seen in the C-terminal domain. In some other nucleases, such as RNase H (Nowotny et al., 2005), a sulfate or phosphate ion is often bound to the apo structure at a site that coincides

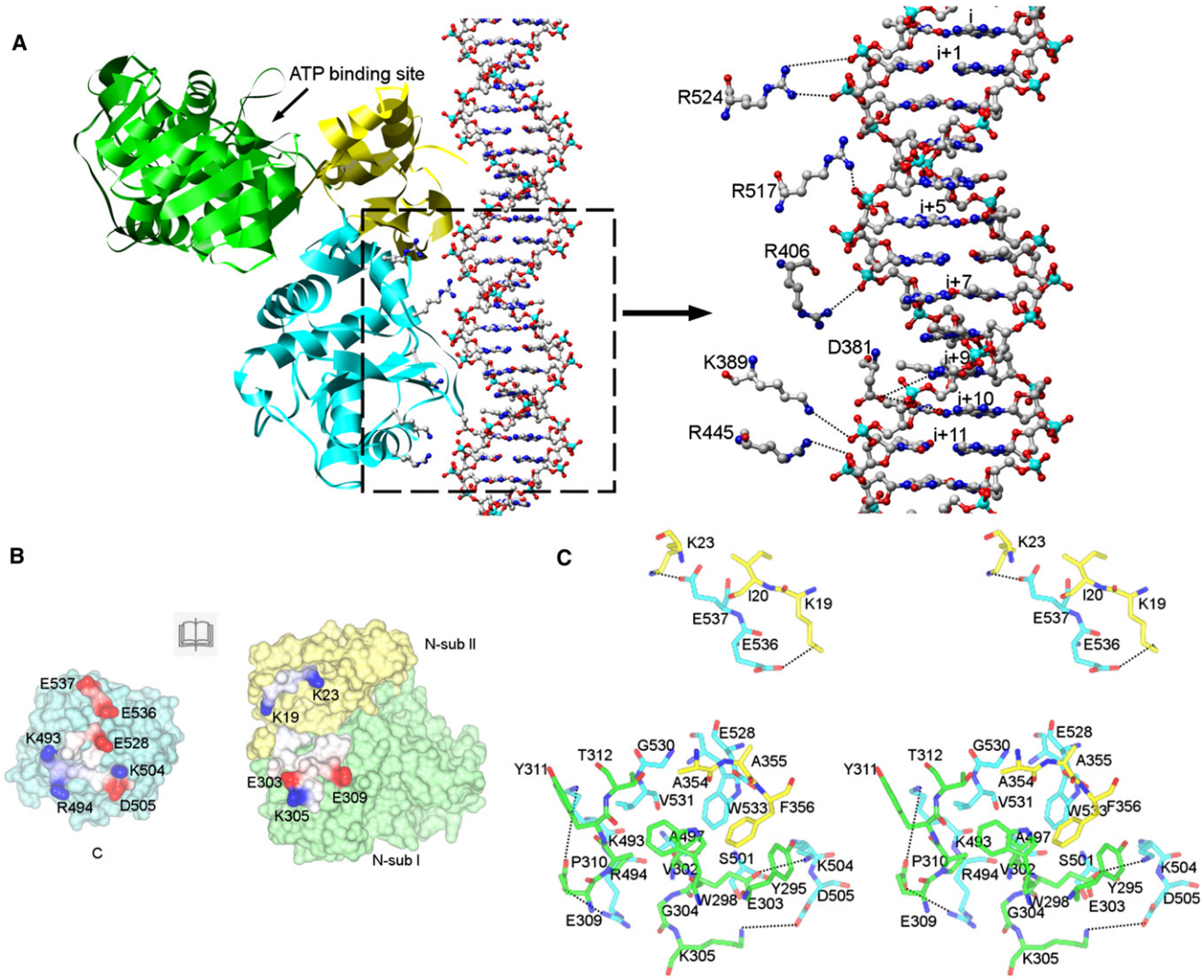

Figure 2. Interactions among the Motor Components during DNA Translocation

In all three panels, gp17 N-terminal subdomain I (N-sub I) is colored green, subdomain II (N-sub II) yellow, and C-terminal domain cyan. (A) was generated with the Chimera program, and (B) and (C) were generated with the CCP4mg program (Potterton et al., 2004).

(A) A model of B-form polyA-polyT DNA molecule is shown bound to the T4 gp17 in the packaging mode. Potential interactions between the gp17 molecule and the DNA are shown as dotted lines in the zoomed view.

(B) Open book view of the gp17 N- and C-terminal domain interactions showing charge complementarity. Positively charged, negatively charged, and hydrophobic surfaces in the contact areas are colored blue, red, and white, respectively. Charged residues in the contact areas are labeled. Contact areas are defined by atoms less than 4.5 Å apart between the N- and C-terminal domains.

(C) Stereo diagram of residues in the N- and C-terminal domains contact areas. Oxygen and nitrogen atoms are colored red and blue, respectively.

with the nucleic acid binding site. A B-form dsDNA was therefore modeled, guided by shape and charge complementarity, such that one of the phosphates on the DNA backbone superimposed on the observed phosphate ion site. The model building showed that residues Arg524, Lys389, and Arg445 could interact with phosphates of DNA bases (*i*, *i* + 1), (*i* + 10), and (*i* + 11) on the "up-strand," and Arg517 and Arg406 could interact with (*i* + 5) and (*i* + 7) on the "down-strand." In addition, a part of the extended loop (amino acids 369–383) could be inserted into the major groove of the DNA, and Asp381 could interact with the nitrogens on bases *i* + 9 and *i* + 10 (Figure 2A). This binding site covers a different area of the C-terminal domain surface from the cutting mode (Figure S5) as described in the previous section and could represent the binding site of dsDNA while it is in a translocation mode.

Arg406 in T4 (Arg403 in RB49) might participate in binding DNA in both the nuclease and the DNA translocation modes. Mutagenesis showed that any amino acid substitution at this position resulted in a null phenotype, producing no plaques (Rentas and Rao, 2003). The R406A mutant retained both "gp16-stimulated ATPase activity" and nuclease activity, suggesting that the mutation did not affect folding. However, it lost

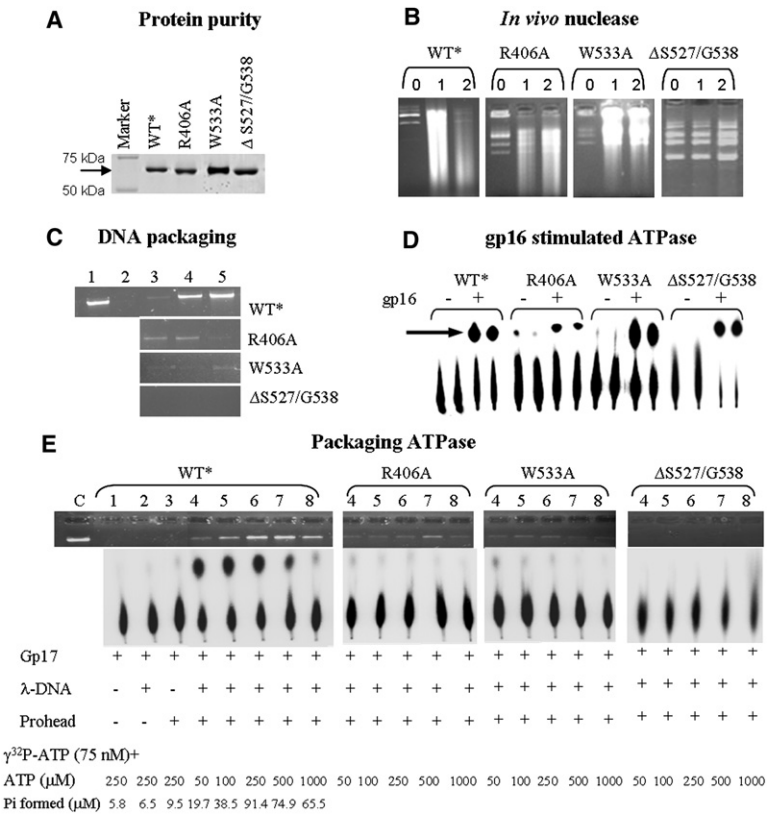

Figure 3. Biochemical Analyses of gp17 Mutants

(A) The wild-type (WT*) and mutant gp17 proteins (R406A, W533A, and ΔS527G538) were purified as described earlier (Kanamaru et al., 2004) and normalized to approximately the same protein concentration for biochemical assays. The WT* and the mutants were truncated by deletion of 33 amino acids at the C terminus because, unlike the full-length gp17, which is susceptible to nonspecific proteolysis during purification, the truncated protein is resistant to proteolysis and retains all the gp17 functions (Kanamaru et al., 2004).

(B) In vivo nuclease assay. Recombinant *E. coli* BL21 (DE3) pLys-S cells containing cloned gp17 constructs were grown, and gp17 expression was induced with isopropyl β-D-1-thiogalactopyranoside (IPTG). Plasmid DNA was isolated and separated by agarose gel electrophoresis and stained with ethidium bromide. Lanes 0, 1, and 2 correspond to plasmid DNA samples at 0, 1, and 2 hr after IPTG induction.

(C) In vitro DNA translocation assay. The DNA translocation activity was assayed by incubating 2×10^9 purified procapsids with gp17, λ DNA (48.5 kb; 300 ng), and ATP. The packaged DNase-resistant DNA was isolated, electrophoresed on an agarose gel, stained with ethidium bromide, and quantified by a Bio-Rad Gel-Doc XR imaging system (Kondabagil et al., 2006). Lane 1, 10% of λ DNA used for packaging; lane 2, gp17 negative control. Lanes 3–5 correspond to 0.5, 1.0, and 1.5 μM of gp17 for WT*, R406A, and W533A; and 1.0, 1.5, and 2 μM of gp17 for ΔS537/G538, respectively.

(D) gp16-stimulated ATPase assay. Each gp17 (0.5 μM) either alone (–) or with gp16 (5 μM) (+) were incubated in duplicate with 1 mM cold ATP and 5 μCi of [γ-^{32}P] ATP (Sp. Act. 3000 Ci/mmol) at 37°C for 20 min. The resultant $^{32}P_i$ was separated by thin layer chromatography and quantified by Phosphor-imaging (Storm 820, Molecular Dynamics) (Leffers and Rao, 2000). The faster migrating spot corresponds to $^{32}P_i$ and is shown with an arrow.

(E) Packaging ATPase assay. The ATPase activity was determined under the defined in vitro DNA packaging conditions in the absence of gp16. The WT* and mutant gp17s (1 μM) were incubated with purified procapsids, λ DNA, and fixed [γ-^{32}P] ATP concentration (75 nM) but increasing cold ATP concentration as shown. This procapsid to gp17 ratio produced no significant ATPase background in the controls (lanes 1–3). The $^{32}P_i$ is low in lanes 7 and 8 because of the large excess of cold ATP.

~90% of DNA translocation activity and "packaging ATPase activity" (Figures 3B–3E). This showed that the DNA binding site is different for translocation and nuclease activity, consistent with the structural observations.

The N-terminal ATPase domain consists of two spatially separated subdomains (Figure 1D) (Sun et al., 2007). The larger subdomain I (amino acids 105–313), the nucleotide binding domain, is connected to subdomain II (residues 1–58 and 314–360) by flexible extended polypeptides. Comparison of the N-terminal domain in its various ligand bound states and when associated with the C-terminal domain shows that the smaller subdomain II can rotate at least 6° relative to subdomain I (Figure S6A). This can introduce a displacement of 3 Å in the linker region between the N- and C-terminal domains. The interface between subdomain I (the ATPase domain) and the C-terminal domain has a 706 Å^2 contact area with four pairs of complimentary charge interactions (Figures 2B and 2C). Similarly, the interface between subdomain II and the C-terminal domain has a 392 Å^2 contact area with two complimentary charge interactions (Figures 2B and 2C). Part of the latter interface involves loop L2 that was disordered in the structure of the C-terminal domain on its own but forms a β-hairpin in the gp17 structure. Trp533, in the L2 loop, is in a hydrophobic environment composed of Tyr295, Trp298, Val302, Ala354, Ala355, and Phe356 in the N-terminal domain, as well as Ala497 and Val531 in the C-terminal domain (Figure 2C).

To analyze the importance of the interdomain interactions, we constructed two mutants, W533A and ΔS527G538. These mutants were predicted to weaken the interactions between the domains by reducing hydrophobic contacts. The W533A mutant has retained "gp16-stimulated ATPase activity" and nuclease activity (Figures 3B and 3D), suggesting that the mutation did not effect folding of either domain. The ΔS527G538 mutant has retained "gp16-stimulated ATPase activity," but has only little nuclease activity, presumably because the deletion is close to Asp539, which is part of the Mg^{2+} binding site. However, both mutants showed almost total loss of DNA translocation activity and "packaging ATPase activity" (Figures 3C and 3E), indicative of the interactions between N- and C-terminal domains being essential for DNA packaging.

The Procapsid-gp17 Cryo-EM Reconstruction

T4 procapsids (Rao and Black, 1985) with bound gp17 are packaging competent in vitro in the absence of the "small terminase" gp16 (Kondabagil et al., 2006). Cryo-EM reconstructions of these procapsids were performed by imposing 5-fold symmetry along

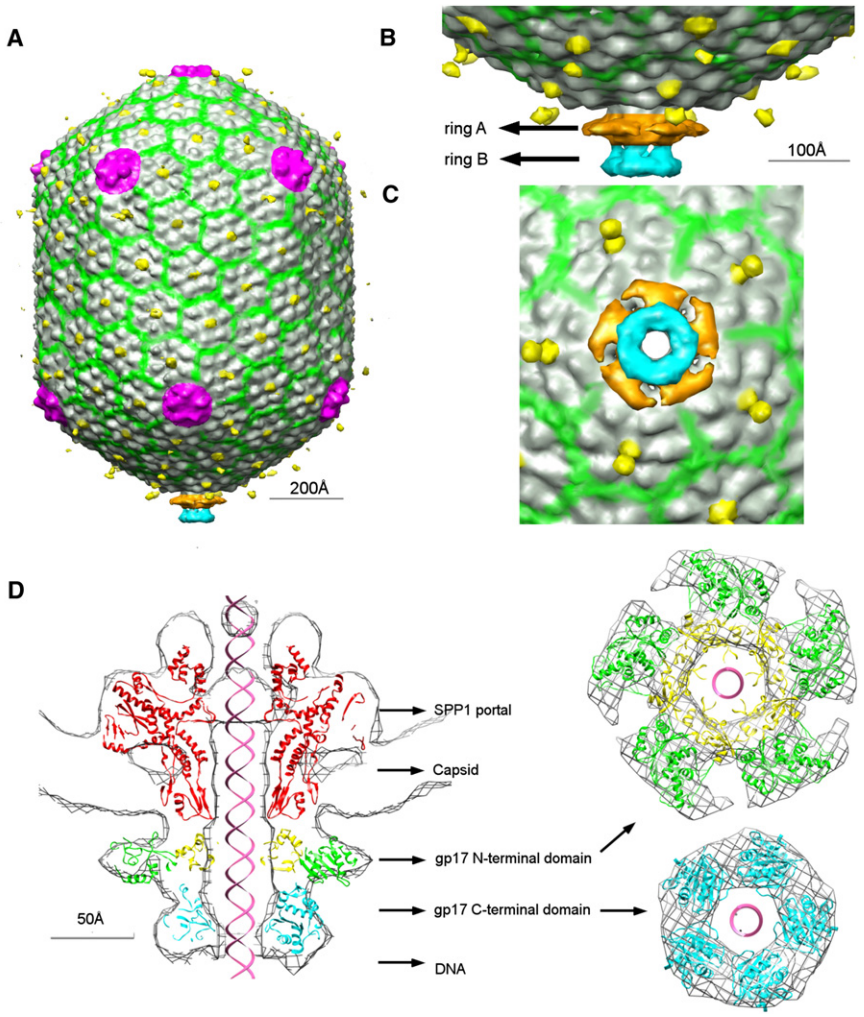

Figure 4. Cryo-EM of T4 Procapsid-gp17 Complex

(A) Cryo-EM map of the T4 procapsid with bound gp17 shows the density for the hexameric capsomers in gray, pentameric capsomers in pink, Hoc proteins in yellow, Soc proteins in green, gp17 N-terminal domain in orange, and C-terminal domain in cyan.

(B) A zoomed in side view shows that the N- and C-terminal domains of gp17 are connected by five short, narrow density regions.

(C) A zoomed in bottom view on the same scale as (B) shows the pentameric distribution of gp17.

(D) Structure of the dodecameric SPP1 portal (red) (based on the crystal structure of the 13-mer) and crystal structures of the N-terminal subdomain I (green), subdomain II (yellow), and C-terminal domain (cyan) of T4 gp17 were fitted into the cryo-EM density. The figure on the left is contoured at 2 σ. All four panels were generated with the Chimera program with the density at 3 σ contour levels unless otherwise stated.

the axis of the particle. As expected, these reconstructions showed the characteristic features of the head with the protruding Hoc molecules at the center of the hexagonal capsomers (Fokine et al., 2004) (Figure 4A and Experimental Procedures). Cryo-EM reconstructions of these procapsids were also performed assuming 6-fold symmetry. To eliminate the dominant 5-fold symmetry of the head, we modified the images by subtraction of the head densities. These modified images were used for both the 5-fold and 6-fold reconstructions. The 5-fold symmetry reconstruction showed well resolved gp17 molecules (see below), whereas the 6-fold averaged reconstruction produced merely smooth donut-shaped rings (Figures 5A and 5B). In addition, a 5-fold averaged cryo-EM reconstruction of procapsids in the act of DNA packaging (Experimental Procedures) showed similar features (Figure 5C). This established that there are five gp17 molecules surrounding the special vertex of the procapsid. Similarly, the DNA packaging machine of ϕ29, which contains a unique 175b RNA (pRNA), had been shown to have five pRNA molecules, each binding one ATPase in a ring

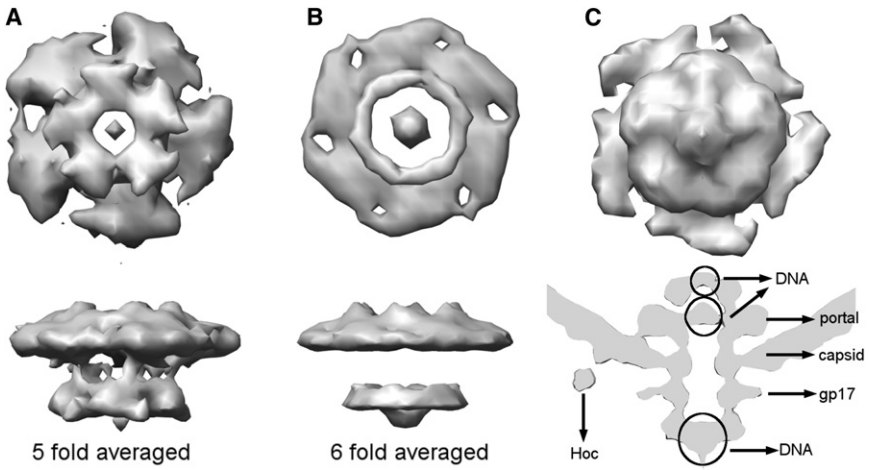

Figure 5. Cryo-EM Reconstructions of gp17 Bound to the Procapsid Assuming 5- or 6-Fold Symmetry

(A) The 5-fold averaged gp17 map shows discrete densities for five gp17 N- and C-terminal domains.

(B) The 6-fold averaged density is much lower, smoother, and featureless. Furthermore, the maximum height of the 6-fold averaged map is only about three-quarters of that of the 5-fold averaged map.

(C) The 5-fold averaged map of the procapsid-gp17 complex while in the process of packaging DNA. The averaged structure of gp17 is seen to be in a relaxed state as might be expected if most of the time there are four gp17 molecules relaxed and one tensed. The reconstruction shows DNA density in the channel formed by the five gp17 molecules and the portal assembly.

around the special vertex (Morais et al., 2001, 2008; Simpson et al., 2000).

Comparison of the 5-fold symmetry imposed reconstructions with and without bound gp17 showed the positions of the portal gp20 and terminase gp17. The T4 gp20 density was fitted with the crystal structure of the SPP1 portal, which is a closer homolog of the T4 portal than the ϕ29 portal is to T4. Two stacked rings below the portal density at the unique vertex presumably correspond to gp17. The ring closer to the head (ring A, Figure 4B) has an external diameter of 160 Å, larger than the 100 Å diameter of ring B farther from the head. At a 3σ contour level, each ring can be separated into five distinct densities, representing five copies of gp17 (Figure 4C). The two rings are connected by five short, narrow density regions (Figure 4B), and ring A is connected to the portal protein (Figure 4D). The symmetry mismatch between gp17 and the 12-fold portal is not likely to form an especially stable contact, as may be required to allow the phage to jettison the packaging machine after completion of DNA packaging, prior to the attachment of the tail. In addition, the interaction between gp17 and the portal is required to form a continuous channel to allow smooth passage of DNA. Mutational data for SPP1 suggests that modifications in the portal protein might alter the property of this channel (Oliveira et al., 2006).

The volume and shape of rings A and B (Figure 4) in the cryo-EM reconstruction show that these represent pentamers of the N- and C-terminal gp17 domains, respectively. However, the structure of the recombinant gp17 consisting of both domains could not be fitted into the cryo-EM density because the N- and C-terminal domains are in close contact with each other in the crystal structure, whereas the cryo-EM density shows separation of the two domains into the A and B rings. Thus, it was concluded that the cryo-EM reconstruction of the procapsid-bound motor is in a "relaxed" pretranslocation state in which the N- and C-terminal domains are well separated from each other.

In contrast to the well separated N- and C-terminal domains observed in the cryo-EM reconstructions, the gp17 crystal structure represents the "tensed," posttranslocation state where the two domains are pulled together, probably by electrostatic forces (Discussion). Thus, the crystal structures of N- and C-terminal domains were separately fitted into their corresponding cryoEM densities with the EMfit program (Rossmann et al., 2001) (Experimental Procedures and Table S2). The resulting relative orientations of the N- and C-terminal domains were the same as the relative orientations of these domains in the full-length ("tensed") crystal structure of gp17 to within 25°. Furthermore, the orientation found for the C-terminal domain placed the proposed DNA translocation binding site facing the center of the channel and would orient DNA bound to this site running parallel to the axis of the phage (Figure 2A). The difference in the center of mass of the C-terminal domain when in a tensed state and when in a relaxed state had a 7.0 Å component along the axis of the head. As the distance between successive base pairs in the DNA structure is 3.4 Å, the distance of the C-terminal domain between the pre- and posttranslocation states is consistent with the packaging of two base pairs per ATP hydrolysis. When gp17 is in the relaxed state, the linker is in an extended conformation. Because flexible portion of proteins often prevent crystal formation, it has only been possible to crystallize gp17 in the tensed form.

The suggestion that gp17 can have a tensed state and a relaxed state is based on two independent observations. The first is that the N- and C-terminal domains in the gp17 crystal structure have more than 1000 Å^2 area of interaction and complementary charge distribution (Figures 2B and 2C), suggesting that the crystal structure is biologically relevant. The second observation is that the cryo-EM reconstruction of the packaging motor consists of two distinct pentameric rings, with the ring closer to the procapsid being the larger and flatter one and, hence, representing the N-terminal domain. However, fitting of the gp17 crystal structure into the appropriate cryo-EM density is not possible. The only reasonable conclusion is that there is a conformational change between the structure observed crystallographically and the structure observed by cryo-EM. Furthermore, the conformational change of gp17 is consistent with the expected translocation of two DNA base pairs produced by the hydrolysis of one ATP molecule and with the DNA translocation binding site on the C-terminal domain of gp17 facing inward toward the DNA.

The Arginine Finger Residue in T4 gp17

In machines that use ATP as fuel, hydrolysis is triggered by the insertion of an "arginine finger" into the active center (Abrahams et al., 1994). By structural comparisons with other ATPases, the controlling Arg in T4 gp17 is Arg162 situated between subdomains I and II on the same (not neighboring) gp17 molecule (Mitchell et al., 2002; Sun et al., 2007) (Figure S7). The accurate positioning of the arginine finger in the active site of the N-terminal ATPase domain could be controlled by the rotation of subdomain II when the C-terminal domain of gp17 binds DNA. The essential character of this arginine residue is evident in that no mutations are tolerated at this position (Rao and Mitchell, 2001). The R162Q and R162K mutants have no significant DNA translocation or "gp16-stimulated ATPase" activities. Furthermore, single turnover ATPase assays show that the mutants are deficient in triggering ATP hydrolysis (Figure S8).

DISCUSSION

The structural information from the crystal structures of gp17, cryo-EM reconstruction of the packaging motor, and the biochemical information based on mutational analyses have made it possible to propose a mechanism for DNA packaging into T4 capsids (Figure 6). In analogy to a car, the N-terminal ATPase subdomain I works as the engine with Arg162, the Arginine finger, acting as a spark plug (see below), and the C-terminal domain corresponds to a car wheel. The N-terminal subdomain II is the gear box that transmits the free energy, liberated when ATP is hydrolysed in the engine, to the C-terminal domain, where the energy is used to translocate the DNA into the capsid. The presence of five gp17 molecules is analogous to a five-cylinder motor.

The Engine of the Packaging Machine

Numerous biological processes use an ATP-fuelled engine. The structure of the most commonly used engine in biological processes is a well known nucleotide binding fold (Rossmann et al., 1974), the most frequently recognizable motif in genome data bases, present in all three domains of life (Chothia et al.,

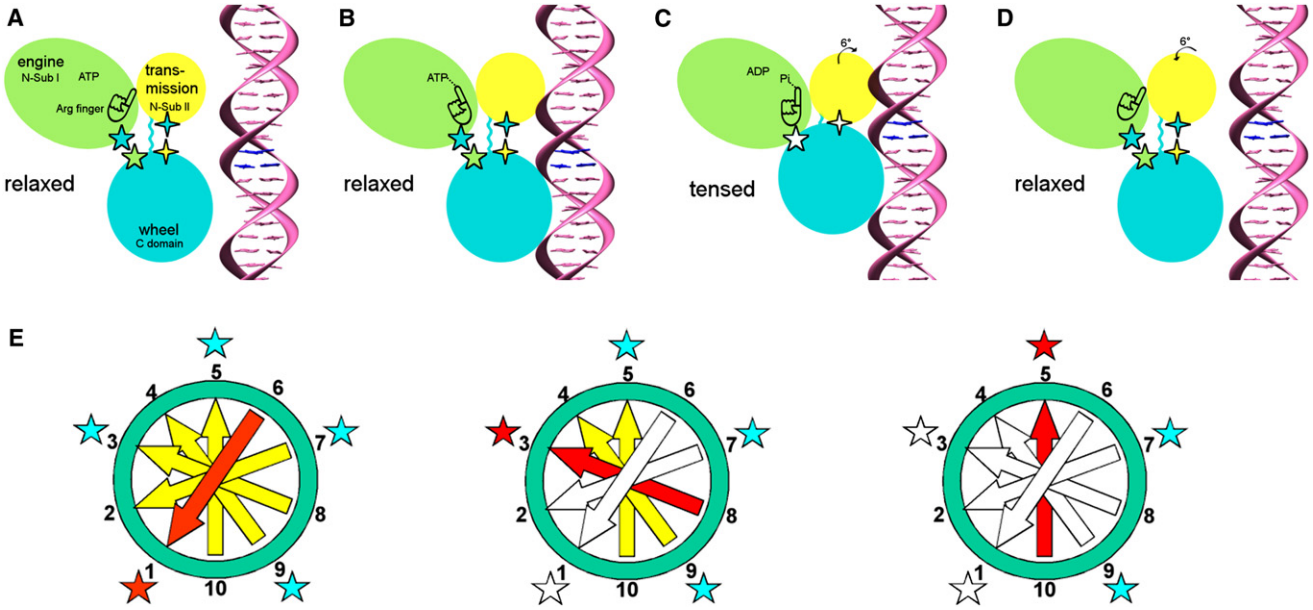

Figure 6. DNA Packaging Mechanism

Panels (A)–(D) relate to the sequence of events that occur in a single gp17 molecule. The gp17 N-terminal subdomain I, subdomain II, and C-terminal domain are represented as green, yellow, and cyan ovals, respectively. The five-pointed stars show the charge interactions between the N-terminal subdomain I and the C-terminal domain. The four-pointed stars show the charge interaction between the N-terminal subdomain II and the C-terminal domain. The flexible linker between N- and C-terminal domain is represented by a wiggly cyan line.

(A) The gp17 C-terminal domain is ready to bind DNA.

(B) The C-terminal domain, when bound to the DNA, brings the DNA closer to the N-terminal domain of the same subunit. Conformational change in the N-terminal domain causes Arg162 to be placed into the ATPase active center in preparation for hydrolysis.

(C) Hydrolysis of ATP has rotated the N-terminal subdomain II by about 6°, thereby aligning the charge pairs resulting in an electrostatic attraction that moves the C-terminal domain and the DNA 6.8 Å (equivalent to the distance between two base pairs) closer to the N-terminal domain and into the capsid.

(D) ADP and Pi are released and the C-terminal domain returns to its original position. DNA is released and is aligned to bind the C-terminal domain of the neighboring subunit.

(E) This panel relates to the synchronization of the five gp17 molecules located around the special vertex of the procapsid. Successive DNA base pairs are indicated by yellow arrows outside the procapsid, red entering the procapsid, and white inside the procapsid. The surrounding five gp17 molecules are shown as stars. The red star represents gp17-ATPase-hydrolyzing ATP, the blue star represents ATPase that is ready to hydrolyze ATP, and the white star represents ATPase that has already hydrolyzed ATP. Left: Hydrolysis of ATP at position 1 translocating two base pairs into the procapsid. Middle: Hydrolysis of ATP at position 3 causing the translocation of further two base pairs into the procapsid. Right: The ATP at position 5 is ready to be hydrolyzed.

2003). The type of work performed by molecular machines is quite variable and is coupled to the engine in ways that are specific for each required function. The coupling must provide a mechanism for suitable transmission of the engine's movements to the required function of the machine, as well as a way of synchronizing the power stroke with the time when the transmission of motion is to occur.

The common nucleotide binding fold for the engine component is the result of evolutionary conservation, indicating that the mechanism of the engine is likely to be the same or similar in ATP-driven motors. In most ATPases that have been studied structurally, the apo enzyme has an "open" conformation that changes to a "closed" conformation when binding ATP (Abrahams et al., 1994; Lee and Yang, 2006). Presumably, the enzyme is oscillating between these conformational states but is stabilized on binding ATP. The loss of free energy on binding will, in part, be converted into heat that raises the possibility of hydrolysis when the ATP is bound in a transition state. ATP hydrolysis breaks the covalent bond between the β and γ phosphates and separates the negatively charged ADP^{3-} and Pi^{3-} molecular remnants. The electrostatic repulsive force between these components reopens the nucleotide binding site and provides the energy for whatever machine, in the current case the DNA translocating machine, is tied to the engine. Once the enzyme has been reopened, the ADP and Pi products can escape. The power stroke could arise from ATP binding as proposed for some RecA-type motors, such as F1 ATPase (Menz et al., 2001), ATP hydrolysis as in kinesin (Rice et al., 1999), or Pi release as in UvrD helicase (Lee and Yang, 2006).

Model for the Packaging Mechanism

In the unliganded pretranslocation relaxed state, the flexible linker between the N- and C-terminal domains is in an extended conformation (Figure 6A). Binding of the dsDNA to the C-terminal domain (Figure 2A) and of an ATP molecule to the N-terminal domain on the same gp17 molecule should cause conformational changes, transmitted by subdomain II, resulting in the insertion of Arg162 (the spark plug) into the ATPase active center to trigger ATP hydrolysis (Figure 6B). As mentioned above, the negatively charged ADP^{3-} and Pi^{3-} products will be mutually repulsed,

causing subdomain II (the transmission domain) to rotate slightly (Figures S6A and S6B), pulling the flexible linker and aligning the charge pairs between the N- and C-terminal domains (Figure 6C). The electrostatic force between opposing charges will pull the C-terminal domain toward the N-terminal domain, thereby translocating two base pairs (Figure 6C). When the ADP^{3-} and Pi^{3-} products are released, there is a net loss of six negative charges, which would attenuate the electrostatic interactions between the N- and C-terminal domains (Figure S6C). In addition, when subdomain II rotates back to its original orientation, the charge pairs between subdomain I and the C-terminal domain would again be misaligned (Figure S6B) and return the C-terminal domain to its original relaxed position (Figure 6D) (Movies S1 and S2). In the meantime, translocation of two base pairs would have placed the neighboring C-terminal domain in the optimal position for binding the dsDNA, as in the previous cycle (see below). Thus, the DNA is handed over from one C-terminal domain to the next by positioning of matching electrostatic interactions between DNA and the binding site in the translocation mode as well as changing DNA binding affinities between relaxed and tensed states. Although there is insufficient information to be certain of the exact moment when the power stroke occurs in the ATP hydrolysis cycle, the above mechanism is the most reasonable interpretation of the available data.

T4 gp17 is monomeric in solution (Kanamaru et al., 2004), consistent with there being little contact between the gp17 molecules in the pseudo-atomic structure of the DNA packaging motor (Figure 4D). Hence, if there is a synchronized sequence of ATP hydrolysis, the information transfer from one gp17 to another most likely occurs through the DNA. This can be achieved by the match of the 10_1 screw symmetry of the dsDNA structure with the 5-fold symmetry of gp17 (Figure 6E). Assuming that, like in ϕ29 (Guo et al., 1987) and T3 (Morita et al., 1993), the motor packages two base pairs per ATP hydrolysis, the gp17 monomer associated with the current ATP being hydrolyzed will have the same structural relationship to bases i and $i + 1$ of the dsDNA as the neighboring gp17 monomer will have to bases $i + 2$ and $i + 3$ after the DNA is translocated by two base pairs into the head. Thus, the relationship of the DNA structure to a specific gp17 monomer should determine the moment when ATP hydrolysis can occur.

Consistent with the mechanism, a mutation that affects DNA binding to the translocation groove (R406A) or mutations that affect N and C domain interface interactions (W533A and ΔS527G538) result in loss of DNA translocation. Also consistent with the mechanism is the conservation, in T4-like phages, of residues involved in the binding of DNA to the translocation binding site in the C-terminal domain and, similarly, of charged residues in the N- and C-terminal domain interface (Figure S9).

At any time during packaging, there should be four gp17 molecules in a relaxed state and one in a tensed state. The 5-fold averaged cryo-EM reconstruction of the procapsid while packaging DNA shows the separated A and B rings, indicating, as expected, that the averaged structure of gp17 is in a relaxed state and that the structure of the procapsid bound gp17 in the absence of DNA is biologically relevant. Since ring B (Figures 4B and 4C) has an inner diameter of about 40 Å, larger than the 23 Å diameter of dsDNA, binding of the gp17 C-terminal domain to dsDNA should be eccentric, with either the specific gp17 C-terminal domain moving toward the center of the channel or the dsDNA moving toward the gp17. However, the latter is more probable because of the discontinuous DNA density in the channel in the cryo-EM reconstruction (Figure 5C).

Contrary to the previous expectations (Simpson et al., 2000), the above DNA packaging mechanism does not involve the portal protein. However, the portal protein is an essential component of the special vertex, acting as an initiator of capsid assembly, providing a platform for attachment of gp17 during packaging and for attachment of the tail upon completion of packaging, and creating a channel for the passage of DNA. In addition, it might also function as a one-way valve preventing the release of packaged DNA between translocation events (Morais et al., 2008).

The above discussions show that the C-terminal domain of gp17 is primarily responsible for DNA translocation. However, another important function of gp17 is to cleave DNA when the head is full (Bhattacharyya and Rao, 1993). The headful signal might be an internal force (Smith et al., 2001) that pops the portal protein further out of the capsid, causing the gp17 packaging motor to dissociate from the capsid and rotate the gp17 molecules to expose their nuclease active surfaces to the DNA.

Comparison with Other Nucleic Acid Packaging Motors

The other well-studied genome packaging motor is for the ssRNA phage ϕ12 (Mancini et al., 2004). The mechanism described here for the T4 DNA packaging motor is dependent on electrostatic forces, whereas the mechanism proposed for the ssRNA packaging motor of phage ϕ12 is based on the mechanical force exerted by loops contacting the ssRNA. The motor in T4 is one of the most powerful molecular machines characterized to date (Fuller et al., 2007). Electrostatic interactions between complimentarily charged ions on two globular protein domains, such as proposed here to occur in the T4 packaging motor, would be capable of generating such a strong force. The driving force of the motor being electrostatic is consistent with the observation that high NaCl concentration interferes with in vitro packaging (V.B.R., unpublished data). Furthermore, in the mechanism for the T4 and presumably ϕ29 dsDNA packaging motors, the synchrony of ATP hydrolysis is determined by the structure of dsDNA whereas, for hexameric ATPases as found in ϕ12, transfer of information would not be easily possible through a structure as flexible as ssRNA (Mancini et al., 2004). Instead, the synchrony is presumably determined by the arginine finger of one subunit interacting directly with the ATPase active center of the neighboring subunit (Abrahams et al., 1994; Mancini et al., 2004). In any of these packaging motors, the subunits hydrolyze ATPs in succession. Thus, blocking one motor subunit by a nonhydrolyzable ATP analog would stall the motor, as was observed in the ϕ29 DNA packaging motor (Chemla et al., 2005).

There has been extensive literature discussing how assembled procapsids of viruses can successfully recognize and package their own genomes (Dube et al., 1993; Hendrix, 1978, 1998; Vale and Milligan, 2000; Valpuesta and Carrascosa, 1994). Biochemical and structural analyses have established that the unique vertices in other dsDNA bacteriophages, such as P22,

ε15, SPP1, and ϕ29, and some eukaryotic viruses, such as herpes viruses, are functionally and structurally similar. Thus, the mechanism for DNA packaging described here for bacteriophage T4, derived from a combination of mutational, biochemical, crystallographic and EM data, is likely to be applicable to these and other dsDNA viruses. More generally, ATP energy conversion into electrostatic forces for mechanical motion of molecules as described here is likely to be a central feature of biological motors.

EXPERIMENTAL PROCEDURES

RB49 gp17 C-Terminal Domain Structure Determination

The RB49 gp17 C-terminal domain (amino acids 358–611) was cloned and purified as described previously (Kanamaru et al., 2004). The protein was concentrated to 10 mg/ml in 20 mM Tris-Cl (pH 8.0) and 100 mM NaCl. Crystals were grown by vapor diffusion in hanging drops at 20°C. Two crystal forms were obtained, one from 15%–20% PEG3350, 0.2M Na/K tartrate with space group $P2_12_12$ and the other from 15% PEG400, 0.2 M KCl, 50 mM Tris (pH 8.5), 10 mM $MgCl_2$ with space group $C2$. For the crystals belonging to space group $P2_12_12$, a heavy atom derivative was prepared by soaking the crystals overnight into mother liquor containing 1 mM ethylmercury phosphate. The diffraction data collection, structure determination, and refinement were done according to standard procedures (Supplemental Experimental Procedures). The structure for the $C2$ space group crystals was determined by molecular replacement with the $P2_12_12$ structure used as a search model and refined with the program CNS (Brünger et al., 1998) (Table 1).

T4 gp17 Structure Determination

The T4 gp17 (amino acids 1–567 with the D255E256/E255D256 mutation) was cloned and purified as described previously (Kanamaru et al., 2004). The protein was concentrated to 10 mg/ml in 20 mM Tris-Cl (pH 8.0) and 100 mM NaCl. Crystals were grown by vapor diffusion in hanging drops at 20°C in 2 M Na/K phosphate (pH 6.0) and 0.1 M CAPS [3-(cyclohexylamino)-1-propane sulfonic acid]. The structure was determined by molecular replacement with the T4 gp17 N-terminal domain and RB49 gp17 C-terminal domain used as search models with the program Phaser (McCoy et al., 2007). Details of the diffraction data collection and structure refinement are given in the Supplemental Experimental Procedures.

Cryo-EM Data Collection and Reconstruction

The phage T4 *17*am*18*am*rII* expanded empty procapsid particles were prepared as previously described (Kondabagil et al., 2006). The gp17 proteins were purified according to the previously described procedure (Kanamaru et al., 2004). Both the purified procapsids and gp17 were highly active for packaging of plasmid DNA in a defined in vitro system (Kondabagil et al., 2006). The procapsid-gp17 complex was prepared by mixing the procapsids and gp17 at a ratio of 100 gp17 molecules to one portal molecule.

An initial procapsid model was constructed on the basis of the knowledge of the mature phage head (Fokine et al., 2004) and used for three-dimensional reconstruction with the program Spider (Frank et al., 1996). Initially, 52 symmetry was assumed and later relaxed to 5-fold symmetry for the final reconstruction. The number of particles incorporated into the procapsid and into the procapsid complexed with gp17 reconstruction were 614 and 1716, giving a final resolution of 37 Å and 34 Å, respectively.

Procapsids in the process of DNA packaging were selected from micrographs taken of particles whose packaging activity had been stopped by adding ATP-γ-S to the reaction mixture about 6 min after initiation. A total of 2001 particles, whose images suggested that they were at least partially filled by DNA, were selected and used in the reconstruction to produce an image at about 32 Å resolution. The resolutions of these reconstructions were determined by the Fourier shell correlation method with a correlation coefficient of 0.5 between independent half data sets as the cutoff criterion.

Fitting of the Atomic Structures into Cryo-EM Density

A three-dimensional orientational search for the best fit of the N-terminal domain structure into ring A of the cryo-EM procapsid reconstruction was restrained (Rossmann et al., 2001) by the knowledge that the C-terminal domain is distal from the capsid (Table S2). The best fit was found to be 2.0 σ above the standard deviation from the mean (σ) taken over the complete three-dimensional search. Similarly, a three-dimensional orientational search for the best fit of the C-terminal domain structure into ring B of the cryo-EM procapsid reconstruction was restrained by the knowledge that the N-terminal domain is proximal to the capsid (Table S2). The best fit was found to be 2.0 σ above the mean.

ACCESSION NUMBERS

The coordinates and associated structure factors have been deposited with the Protein Data Bank (accession numbers 3C6A for RB49 gp17 C-terminal domain space group $P2_12_12$, 3C6H for $C2$, 3CPE for T4 gp17, and 3EZK for the pentameric T4 gp17 model from EMfit). The cryo-EM maps have been deposited with the Electron Microscopy Data Bank (accession codes EMD-1572 for T4 procapsid-gp17 complex and EMD-1573 for T4 procapsid in the process of DNA packaging).

SUPPLEMENTAL DATA

Supplemental Data include Supplemental Experimental Procedures, nine figures, two tables, and two movies and can be found with this article online at http://www.cell.com/supplemental/S0092-8674(08)01447-5.

ACKNOWLEDGMENTS

We thank Petr Leiman, Ping Zhang, Ye Xiang, Paul Chipman, and especially Victor Kostyuchenko for helpful advice on cryo-EM reconstruction. We also thank Anastasia Aksyuk, Petr Leiman, and William Cramer for discussions on the mechanisms of ATP-driven motors. We are grateful to David Stuart, Marc Morais, Petr Leiman, and Bentley Fane for reading and commenting on the manuscript. We thank Sheryl Kelly and Cheryl Towell for help in the preparation of the manuscript. We also thank the staff of the Advanced Photon Source, The General Medicine and Cancer Institutes sector for their help in X-ray diffraction data collection, whose facilities are supported by the U.S. Department of Energy and the National Institutes of Health. This work was supported by National Science Foundation grants to M.G.R (MCB-443899) and V.B.R (MCB-423528).

Received: April 28, 2008
Revised: September 18, 2008
Accepted: November 3, 2008
Published: December 24, 2008

REFERENCES

Abrahams, J.P., Leslie, A.G.W., Lutter, R., and Walker, J.E. (1994). Structure at 2.8 Å resolution of F1-ATPase from bovine heart mitochondria. Nature *370*, 621–628.

Alam, T.I., Draper, B., Kondabagil, K., Rentas, F.J., Ghosh-Kumar, M., Sun, S., Rossmann, M.G., and Rao, V.B. (2008). The headful packaging nuclease of bacteriophage T4. Mol. Microbiol. *69*, 1180–1190.

Baumann, R.G., Mullaney, J., and Black, L.W. (2006). Portal fusion protein constraints on function in DNA packaging of bacteriophage T4. Mol. Microbiol. *61*, 16–32.

Beese, L.S., and Steitz, T.A. (1991). Structural basis for the 3′-5′ exonuclease activity of *Escherichia coli* DNA polymerase I: a two metal ion mechanism. EMBO J. *10*, 25–33.

Bhattacharyya, S.P., and Rao, V.B. (1993). A novel terminase activity associated with the DNA packaging protein gp17 of bacteriophage T4. Virology *196*, 34–44.

Black, L.W. (1989). DNA packaging in dsDNA bacteriophages. Annu. Rev. Microbiol. *43*, 267–292.

Brünger, A.T., Adams, P.D., Clore, G.M., DeLano, W.L., Gros, P., Grosse-Kunstleve, R.W., Jiang, J.S., Kuszewski, J., Nilges, M., Pannu, N.S., et al. (1998). *Crystallography and NMR system*: a new software suite for macromolecular structure determination. Acta Crystallogr. D Biol. Crystallogr. *54*, 905–921.

Chang, J., Weigele, P., King, J., Chiu, W., and Jiang, W. (2006). Cryo-EM asymmetric reconstruction of bacteriophage P22 reveals organization of its DNA packaging and infecting machinery. Structure *14*, 1073–1082.

Chemla, Y.R., Aathavan, K., Michaelis, J., Grimes, S., Jardine, P.J., Anderson, D.L., and Bustamante, C. (2005). Mechanism of force generation of a viral DNA packaging motor. Cell *122*, 683–692.

Chothia, C., Gough, J., Vogel, C., and Teichmann, S.A. (2003). Evolution of the protein repertoire. Science *300*, 1701–1703.

Dube, P., Tavares, P., Lurz, R., and van Heel, M. (1993). The portal protein of bacteriophage SPP1: a DNA pump with 13-fold symmetry. EMBO J. *12*, 1303–1309.

Fokine, A., Chipman, P.R., Leiman, P.G., Mesyanzhinov, V.V., Rao, V.B., and Rossmann, M.G. (2004). Molecular architecture of the prolate head of bacteriophage T4. Proc. Natl. Acad. Sci. USA *101*, 6003–6008.

Frank, J., Radermacher, M., Penczek, P., Zhu, J., Li, Y., Ladjadj, M., and Leith, A. (1996). SPIDER and WEB: processing and visualization of images in 3D electron microscopy and related fields. J. Struct. Biol. *116*, 190–199.

Fuller, D.N., Raymer, D.M., Kottadiel, V., Rao, V.B., and Smith, D.E. (2007). Single phage T4 DNA packaging motors exhibit large force generation, high velocity, and dynamic variability. Proc. Natl. Acad. Sci. USA *104*, 16868–16873.

Guo, P., Peterson, C., and Anderson, D.L. (1987). Prohead and DNA-gp3-dependent ATPase activity of the DNA packaging protein gp16 of bacteriophage ϕ29. J. Mol. Biol. *197*, 229–236.

Hendrix, R.W. (1978). Symmetry mismatch and DNA packaging in large bacteriophages. Proc. Natl. Acad. Sci. USA *75*, 4779–4783.

Hendrix, R.W. (1998). Bacteriophage DNA packaging: RNA gears in a DNA transport machine. Cell *94*, 147–150.

Hugel, T., Michaelis, J., Hetherington, C.L., Jardine, P.J., Grimes, S., Walter, J.M., Falk, W., Anderson, D.L., and Bustamante, C. (2007). Experimental test of connector rotation during DNA packaging into bacteriophage ϕ29 capsids. PLoS Biol. *5*, e59.

Jiang, W., Chang, J., Jakana, J., Weigele, P., King, J., and Chiu, W. (2006). Structure of epsilon15 bacteriophage reveals genome organization and DNA packaging/injection apparatus. Nature *439*, 612–616.

Kanamaru, S., Kondabagil, K., Rossmann, M.G., and Rao, V.B. (2004). The functional domains of bacteriophage T4 terminase. J. Biol. Chem. *279*, 40795–40801.

Kondabagil, K.R., Zhang, Z., and Rao, V.B. (2006). The DNA translocating ATPase of bacteriophage T4 packaging motor. J. Mol. Biol. *363*, 786–799.

Lander, G.C., Tang, L., Casjens, S.R., Gilcrease, E.B., Prevelige, P., Poliakov, A., Potter, C.S., Carragher, B., and Johnson, J.E. (2006). The structure of an infectious P22 virion shows the signal for headful DNA packaging. Science *312*, 1791–1795.

Lebedev, A.A., Krause, M.H., Isidro, A.L., Vagin, A.A., Orlova, E.V., Turner, J., Dodson, E.J., Tavares, P., and Antson, A.A. (2007). Structural framework for DNA translocation via the viral portal protein. EMBO J. *26*, 1984–1994.

Lee, J.Y., and Yang, W. (2006). UvrD helicase unwinds DNA one base pair at a time by a two-part power stroke. Cell *127*, 1349–1360.

Leffers, G., and Rao, V.B. (2000). Biochemical characterization of an ATPase activity associated with the large packaging subunit gp17 from bacteriophage T4. J. Biol. Chem. *275*, 37127–37136.

Leiman, P.G., Chipman, P.R., Kostyuchenko, V.A., Mesyanzhinov, V.V., and Rossmann, M.G. (2004). Three-dimensional rearrangement of proteins in the tail of bacteriophage T4 on infection of its host. Cell *118*, 419–429.

Mancini, E.J., Kainov, D.E., Grimes, J.M., Tuma, R., Bamford, D.H., and Stuart, D.I. (2004). Atomic snapshots of an RNA packaging motor reveal conformational changes linking ATP hydrolysis to RNA translocation. Cell *118*, 743–755.

McCoy, A.J., Grosse-Kunstleve, R.W., Adams, P.D., Winn, M.D., Storoni, L.C., and Read, R.J. (2007). *Phaser* crystallographic software. J. Appl. Cryst. *40*, 658–674.

Menz, R.I., Walker, J.E., and Leslie, A.G.W. (2001). Structure of bovine mitochondrial F_1-ATPase with nucleotide bound to all three catalytic sites. Cell *106*, 331–341.

Mitchell, M.S., Matsuzaki, S., Imai, S., and Rao, V.B. (2002). Sequence analysis of bacteriophage T4 DNA packaging/terminase genes 16 and 17 reveals a common ATPase center in the large subunit of viral terminases. Nucleic Acids Res. *30*, 4009–4021.

Morais, M.C., Tao, Y., Olson, N.H., Grimes, S., Jardine, P.J., Anderson, D.L., Baker, T.S., and Rossmann, M.G. (2001). Cryoelectron-microscopy image reconstruction of symmetry mismatches in bacteriophage ϕ29. J. Struct. Biol. *135*, 38–46.

Morais, M.C., Koti, J.S., Bowman, V.D., Reyes-Aldrete, E., Anderson, D.L., and Rossmann, M.G. (2008). Defining molecular and domain boundaries in the bacteriophage ϕ29 DNA packaging motor. Structure *16*, 1267–1274.

Morita, M., Tasaka, M., and Fujisawa, H. (1993). DNA packaging ATPase of bacteriophage T3. Virology *193*, 748–752.

Nowotny, M., Gaidamakov, S.A., Crouch, R.J., and Yang, W. (2005). Crystal structures of RNase H bound to an RNA/DNA hybrid: substrate specificity and metal-dependent catalysis. Cell *121*, 1005–1016.

Oliveira, L., Henriques, A.O., and Tavares, P. (2006). Modulation of the viral ATPase activity by the portal protein correlates with DNA packaging efficiency. J. Biol. Chem. *281*, 21914–21923.

Orlova, E.V., Gowen, B., Dröge, A., Stiege, A., Weise, F., Lurz, R., van Heel, M., and Tavares, P. (2003). Structure of a viral DNA gatekeeper at 10 Å resolution by cryo-electron microscopy. EMBO J. *22*, 1255–1262.

Pettersen, E.F., Goddard, T.D., Huang, C.C., Couch, G.S., Greenblatt, D.M., Meng, E.C., and Ferrin, T.E. (2004). UCSF Chimera-a visualization system for exploratory research and analysis. J. Comput. Chem. *25*, 1605–1612.

Potterton, L., McNicholas, S., Krissinel, E., Gruber, J., Cowtan, K., Emsley, P., Murshudov, G.N., Cohen, S., Perrakis, A., and Noble, M. (2004). Developments in the CCP4 molecular-graphics project. Acta Crystallogr. D Biol. Crystallogr. *60*, 2288–2294.

Rao, V.B., and Black, L.W. (1985). DNA packaging of bacteriophage T4 proheads in vitro evidence that prohead expansion is not coupled to DNA packaging. J. Mol. Biol. *185*, 565–578.

Rao, V.B., and Black, L.W. (2005). DNA packaging in bacteriophage T4. In Viral Genome Packaging Machines: Genetics, Structure, and Mechanism, C.E. Catalano, ed. (Georgetown, TX: Landes Bioscience), pp. 40–58.

Rao, V.B., and Feiss, M. (2008). The bacteriophage DNA packaging motor. Annu. Rev. Genet. *42*, 647–781.

Rao, V.B., and Mitchell, M.S. (2001). The N-terminal ATPase site in the large terminase protein gp17 is critically required for DNA packaging in bacteriophage T4. J. Mol. Biol. *314*, 401–411.

Rentas, F.J., and Rao, V.B. (2003). Defining the bacteriophage T4 DNA packaging machine: evidence for a C-terminal DNA cleavage domain in the large terminase/packaging protein gp17. J. Mol. Biol. *334*, 37–52.

Rice, S., Lin, A.W., Safer, D., Hart, C.L., Naber, N., Carragher, B.O., Cain, S.M., Pechatnikova, E., Wilson-Kubalek, E.M., Whittaker, M., et al. (1999). A structural change in the kinesin motor protein that drives motility. Nature *402*, 778–784.

Rossmann, M.G., Moras, D., and Olsen, K.W. (1974). Chemical and biological evolution of a nucleotide-binding protein. Nature *250*, 194–199.

Rossmann, M.G., Bernal, R., and Pletnev, S.V. (2001). Combining electron microscopic with X-ray crystallographic structures. J. Struct. Biol. *136*, 190–200.

Simpson, A.A., Tao, Y., Leiman, P.G., Badasso, M.O., He, Y., Jardine, P.J., Olson, N.H., Morais, M.C., Grimes, S., Anderson, D.L., et al. (2000). Structure of the bacteriophage ϕ29 DNA packaging motor. Nature *408*, 745–750.

Smith, D.E., Tans, S.J., Smith, S.B., Grimes, S., Anderson, D.L., and Bustamante, C. (2001). The bacteriophage ϕ29 portal motor can package DNA against a large internal force. Nature *413*, 748–752.

Streisinger, G., Emrich, J., and Stahl, M.M. (1967). Chromosome structure in phage T4, III. terminal tedundancy and length determination. Proc. Natl. Acad. Sci. USA *57*, 292–295.

Sun, S., Kondabagil, K., Gentz, P.M., Rossmann, M.G., and Rao, V.B. (2007). The structure of the ATPase that powers DNA packaging into bacteriophage T4 procapsids. Mol. Cell *25*, 943–949.

Vale, R.D., and Milligan, R.A. (2000). The way things move: looking under the hood of molecular motor proteins. Science *288*, 88–95.

Valpuesta, J.M., and Carrascosa, J.L. (1994). Structure of viral connectors and their function in bacteriophage assembly and DNA packaging. Q. Rev. Biophys. *27*, 107–155.